Effect of suspended TiO$_2$ physicochemical characteristics on benzene derivatives photocatalytic degradation

D. Gumy [a], S.A. Giraldo [c], J. Rengifo [b], C. Pulgarin [b],*

[a] Institute of Environmental Science and Technology, LBE, EPFL, Switzerland
[b] Institute of Chemical Science and Engineering, GGEC, EPFL, Station 6, CH-1015 Lausanne, Switzerland
[c] Centro de Investigaciones en catálisis (CICAT), Escuela de Ingeniería Química,
Universidad Industrial de Santander (UIS), Cra. 27 calle 9, Bucaramanga, Colombia

Abstract

Seven different TiO$_2$ samples suitable for water detoxification were systematically characterized according to their physicochemical properties. Except for one mixed catalyst anatase–rutile from Degussa P25, all photocatalysts had a pure anatase crystalline phase. The particle size of the TiO$_2$ samples varied from about 5 to 700 nm and was inversely correlated with the BET specific surface area (A_{BET}). Surface properties of colloidal suspensions measured by electroacoustic methods were evaluated at different pH values. The aggregate size appeared to be dependent on the pH value of the solution. The isoelectric point (IEP) of the TiO$_2$ samples ranged from very acidic (IEP < 3) to neutral values.

Four benzene derivatives were chosen as model pollutants to assess the TiO$_2$ samples efficiency on water detoxification.

The organic degradation kinetics were influenced in a different way by the TiO$_2$ characteristics. The surface charge of TiO$_2$ samples was found to affect significantly the organic degradation kinetics. Indeed, the compounds degradation was greatly enhanced by acidic TiO$_2$. Moreover, the compounds primary degradation and the total mineralization were affected differently by the A_{BET}. The primary degradation kinetics of strongly adsorbed pollutants, i.e. those containing a carboxyl group, benzoic acid (BA) and 4-hydroxybenzoic acid (HBA), is enhanced by large A_{BET}, whereas phenol and 4-nitrophenol (NP) degradation was not. On the other hand, a small A_{BET} was not advantageous, and there is an optimum value for an efficient total organic carbon (TOC) removal. In addition, the mixed crystalline structure, Degussa P25, showed a higher photoactivity than pure anatase TiO$_2$, as generally accepted and reported in previous studies.
© 2007 Elsevier B.V. All rights reserved.

Keywords: Water detoxification; TiO$_2$ photoactivity; Benzoic acid; 4-Hydrobenzoic acid; Phenol; 4-Nitrophenol

1. Introduction

The photocatalytic water treatment with TiO$_2$ efficiently destroys many organic pollutants [1]. The photocatalytic degradation rate of different compounds depends on various parameters, such as temperature, pH, pollutant initial concentration, TiO$_2$ concentration, light intensity, chemical nature (structure) of the reactant, TiO$_2$ physicochemical characteristics, and optical properties of the TiO$_2$, especially when the catalyst particles are suspended in aqueous solution.

Schematically, dissolved organic molecules can either react on the surface of the solid in the case of adsorption or in solution when they are neither adsorbed nor chemisorbed. However, OH$^\bullet$ and/or holes are considered as the main oxidative species responsible for organic oxidation, and it is well known that organic adsorption is a prerequisite for a highly efficient photodegradation.

The formation rate of oxidative surface species is known to be a function of the particle size, aggregate size in suspension, crystalline phase, crystallinity and other nano-structural parameters [2–4].

Experimental investigations on the influence of the particle size on the TiO$_2$ photoactivity showed that there is an optimum TiO$_2$ particle size for which the photocatalytic oxidation rates of organic substrates are maximized [5–8].

Both crystal structures, anatase and rutile, are commonly used as photocatalysts, with anatase showing a greater photocatalytic activity for most reactions. It has been suggested

that this increased photoreactivity is due to the anatase slightly higher Fermi level, lower capacity to adsorb oxygen and higher degree of hydroxylation (i.e. number of hydroxyl groups on the surface). However, some studies showed that a mixture of anatase (70–75%) and rutile (30–25%) is more active than pure anatase [9,10]. The behaviour of Degussa P25 commercial TiO$_2$ photocatalyst, consisting of an amorphous state with a mixture of anatase and rutile in an approximate proportion of 70/30, is for many reactions more active than both pure crystalline phases [10,11]. Crystallinity of TiO$_2$ was experimentally shown to be an important factor in presenting a high photocatalytic activity for the decomposition of pollutants in water [12,13].

The TiO$_2$ adsorption capacity is influenced by its specific surface area [14]. The transfer of the reactants in the liquid phase to the TiO$_2$ surface and their adsorption are influenced by the catalyst surface charge, and therefore, by its zero point charge or isoelectric point IEP [15,16].

Various studies have reported that the photocatalytic reactivity of aromatic compounds can be affected by the number of substituents, their electronic nature, and their positions in the aromatic ring [17–21]. However, few studies correlate the measured photodegradation rates with the characteristics of the compounds to be degraded [22]. The photocatalytic degradability of some compounds has been principally correlated to the Hammett constant (σ) and to the 1-octanol–water partition coefficient (K_{ow}). The σ describes the effect of the different substituents on the electronic character of a given aromatic system. A positive σ value indicates an electron-withdrawing group, while a negative value indicates an electron-donating group [22].

K_{ow} reflects the hydrophobicity, i.e. the tendency of these molecules to remain in or escape from water, and can be related to the extent of the organic compound adsorption on TiO$_2$. The adsorption of organic compounds depends on their hydrophobic character, and a low value of K_{ow} indicates a weak affinity of the compound for the TiO$_2$ particles dispersed in water [23].

The pH of an aqueous solution significantly affects all oxide semiconductors including the surface charge of the semiconductor particles, the aggregates size and the conduction and valence bands energies. The pH influences at the same time both the surface state of titania and the ionization state of ionizable organic molecules. For pH values higher than the IEP of titania, the surface becomes negatively charged and positively charged for pH < IEP, according to the following equilibrium:

$$pH < IEP : Ti-OH + H^+ \Leftrightarrow TiOH_2^+ \qquad (1)$$

$$pH > IEP : Ti-OH + OH^- \Leftrightarrow TiO^- + H_2O \qquad (2)$$
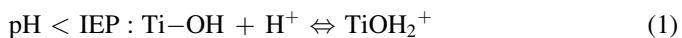
Thus, electrostatic attraction–repulsion effects will influence the mechanisms of adsorption and desorption of organic compounds onto TiO$_2$. Some anions commonly found in natural or polluted waters (e.g., chloride, bromide, sulphate, phosphate, carbonate) have an inhibiting effect on the photodegradation process if they are bound to TiO$_2$ or close to its surface [24–26]. Consequently, pH and IEP are determinant for the effect of ions, as are the chemical affinities

of the ions for TiO$_2$. For instance, a significant degradation rate inhibition of different compounds has been observed in presence of chloride at pH 3 [27]. At acidic pH, TiOH$_2^+$ and TiOH are the main species on the catalyst surface (Eq. (1)), and the chloride ions compete with the organic compounds for the active sites, thus, lowering the degradation rates. At higher pH, the negatively charged catalyst surface (Eq. (2)) repulses the chloride ions and no inhibiting effect is observed.

Moreover, the optical properties of the suspended catalysts can have a significant influence on their photocatalytic activities. Indeed, the TiO$_2$ particles suspended in the liquid phase cause scattering and absorption phenomena. Only the absorbed radiation can induce photocatalysis, while scattering is detrimental to it [28]. Recent studies reported that TiO$_2$ with larger particles and lower surface area performed better in the degradation of phenol than TiO$_2$ with smaller particles and larger surface area [29,30]. This behaviour was attributed to a lower scattering in the UV range of the photocatalysts having larger particles.

The objective of this work is to obtain a detailed characterization of seven samples of different TiO$_2$ commercial powders and relate their properties with the kinetics of degradation of some phenolic water contaminants. The type and source of TiO$_2$ selected for the photocatalysis plays an important role in the contaminant removal, since the rate of formation of the oxidative surface species and the interaction between contaminants and TiO$_2$ depends on physicochemical characteristics of the TiO$_2$ type. The main characteristics influencing the TiO$_2$ activity are the particle size, the aggregate size in suspension, the A_{BET}, the IEP, the crystalline phase, the crystallinity, and the surface density of OH groups [3,4].

2. Experimental

2.1. TiO$_2$ samples and characterization

The TiO$_2$ samples were provided by Degussa AG (P25), Millennium Chemicals (PC10, PC50, PC500), Tayca samples of Mitsubishi Int. Corp. (JA1, TKS201, TKS203). The addresses of these suppliers are found in the acknowledgment section.

The characteristics of the seven TiO$_2$ are listed in Table 1. They were measured according to the methods reported by Gumy et al. [31].

2.2. Chemicals and analysis

Phenol, catechol, resorcinol, hydroquinone, 4-hydroxybenzoic acid, and 4-nitrophenol were obtained from Fluka.

The chemicals for high-performance liquid chromatography (HPLC) analysis were obtained from Acros Organics. Milli-Q water was used throughout for the preparation of aqueous solutions or as a component of the mixed water–acetonitrile (HPLC grade) mobile phase in HPLC analysis. In all cases, the concentration of pollutants and their main degradation intermediates was measured with a chromatograph Varian 9065 Unit, equipped with a diode array (Varian, Switzerland).

Table 1
Characteristics of TiO_2 samples used in detoxification experiments at pH 6

Type of TiO_2	Crystalline phase	IEP	A_{BET} (m²/g)	Particle size (nm)	Aggregate radius (nm)
Degussa P25	Anatase–rutile	7.0	56	25–35	370
Millennium PC10	Anatase	5.7	10	70	1000
Millennium PC50	Anatase	6.8	50	20–30	8200
Millennium PC500	Anatase	6.2	335	5–10	1400
Tayca TKS201	Anatase	7.5	214	6	130
Tayca TKS203	Anatase	<3	241	6	200
Tayca JA1	Anatase	<3	9	180	9200

IEP: isoelectric point; A_{BET}: BET specific surface area.

A spheriosorb silica column (ODS-2) of 250 mm length and 4.6 mm diameter was used. The eluent was either a mixture of acetonitrile/water or acetonitrile/acetic acid (10%, v/v), and a gradient elution from 5 to 80% of acetonitrile was used.

A Shimadzu, model 5050A, TOC analyzer was used for total organic carbon (TOC) measurements. The instrument was equipped with an automatic sample injector (ASI) and potassium phthalate solution was used as calibration standard. Acidification and stripping before analysis were sometimes necessary to keep the solutions free of atmospheric CO_2.

2.3. Photocatalysis experiments

Four different compounds were chosen for this study: phenol, benzoic acid (BA), 4-nitrophenol (NP) and 4-hydroxybenzoic acid (HBA). Their physicochemical characteristics are summarized in Table 2.

The photocatalytic experiments were performed using Pyrex glass containers of 50 ml (3 cm in diameter and 5 cm high) closed with septa as cylindrical batch photoreactors. Illumination was performed with a xenon lamp in a CPS Suntest system (Atlas GmbH) at 550 W/m² light intensity (AM1) with a filter that cuts off wavelengths below 290 nm. The total radiant flux was measured with a Kipp & Zonen (CM3) power meter. The lamp had a λ distribution with about 0.5% of the emitted photons at wavelengths shorter than 300 nm and about 7% between 300 and 400 nm. The profile of the photons emitted between 400 and 800 nm followed the solar spectrum. TiO_2 concentration of 1.0 g/l was used during experiments. The appropriate TiO_2 sample was used for each run and the pH value was not adjusted but measured at the beginning and at the end of each experiment. At the beginning of the experiments, while reactors were kept in the dark, a chosen benzoic compound was added at a concentration of 0.5 mM and the reactor was

magnetically stirred. Samples were first collected at predetermined times in the dark; then, the solar lamp was turned on, and samples were collected at predetermined times during 4 h.

The aqueous pollutant solutions and TiO_2 suspensions were magnetically stirred throughout irradiation, opened to air. Extreme care was taken to ensure uniform experimental conditions during the degradation rate determination. The disappearance of each substance was monitored by HPLC after catalyst removal through filtration with Millipore filters (0.45 μm). The results of the organics degradation at preselected photocatalysis times were averaged over three experimental points.

3. Results and discussion

3.1. Phenol

There is a large debate on whether titanium dioxide preparations commercially available are the most efficient as photocatalysts. Together with various characteristics such as particle size, crystalline form or active site density, which may intervene in the photocatalytic activity, the influence of the catalyst surface area appeared to be of prime importance because it is generally correlated with its pollutant adsorption capacity [16,32].

Fig. 1 shows the phenol concentration evolution as a function of time during photocatalytic experiments with seven
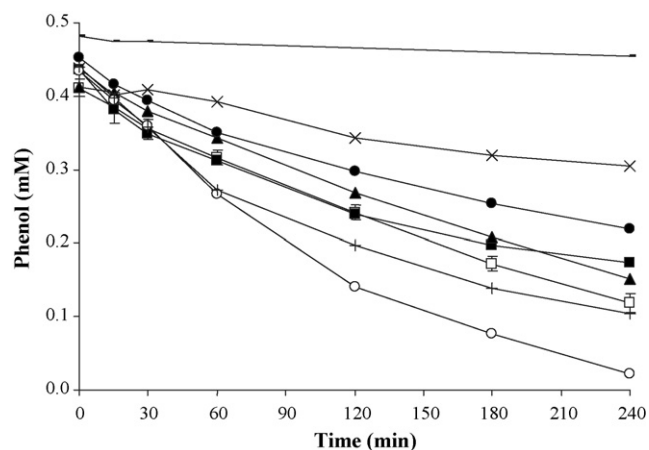
Table 2
Characteristics of benzene derivatives

Benzoic compounds	MM (g/mol)	pH[a] (0.5 mM)	pK_a	log K_{ow}	σ[b] Hammet
Phenol	94	5.7	9.99	1.46	0.00
Benzoic acid	122	3.8	4.19	1.50	0.63
4-Nitrophenol	139	4.9	7.15	1.86	0.81
4-Hydroxybenzoic acid	138	4.0	4.57	1.37	0.44

[a] Before TiO_2 addition.
[b] Relative to phenol.

Fig. 1. Photodegradation of phenol (0.5 mM) with different TiO_2 in suspension (1 g/l): P25 (□), Millennium PC10 (■), PC50 (▲), PC500 (×), Tayca JA1 (+), TKS201 (●), TKS203 (○) and without TiO_2 addition (–) as a function of time. Light intensity of 550 W/m².

Table 3
Apparent first-order rate constant k for phenol disappearance with the different TiO$_2$ samples and their corresponding global correlation coefficient R^2 value

	TiO$_2$ samples						
	TKS 203	JA1	P25	PC10	PC50	TKS 201	PC500
k (min^{-1})	0.562	0.377	0.297	0.257	0.218	0.192	0.101
R^2	0.99	0.99	0.99	0.95	0.97	0.99	0.93

different TiO$_2$ samples tested at a concentration of 1.0 g/l and a light intensity of 550 W/m^2, as well as the effect of the light without catalyst. Their respective first-order rate constants are listed in Table 3. The experimental errors were calculated for all the TiO$_2$ samples. Representative errors bars are displayed only on the P25 TiO$_2$ plot. The average error was below 5% for repetitions of phenol and TOC removal experiments with the different TiO$_2$.

Preliminary adsorption experiments performed until 24 h in the dark have demonstrated that the equilibrium is already reached after 1 h (results not shown). Adsorption in the dark (time range of −60 to 0 min) was carried out for all catalysts. It appears that the phenol adsorption is not correlated with the catalyst A_{BET} or with IEP (Fig. 1 and Table 1), and that phenol is poorly adsorbed onto TiO$_2$, as reported previously [33–36]. The two TiO$_2$ samples with an average specific surface area ($A_{BET} \approx 50$ m^2/g) and a neutral IEP, P25 and PC50, present the highest adsorption capacity. Moreover, catalysts with very different A_{BET}, from 10 m^2/g (PC10 and JA1) to more than 200 m^2/g (PC500, TKS201 and TKS203), showed approximately the same adsorption capacity. Catalysts with IEP varying from acidic (TKS203 and JA1) to neutral (PC10, TKS201 and PC500) value showed also very similar quantity of phenol absorbed on their surface.

For all experiments, the pH was measured first directly after addition of the different TiO$_2$ in the 0.5 mM phenol solution, then after 1 h of darkness adsorption and, finally at the end of the experiment (see Table 4). The measured pH was always below the pK_a of phenol (9.99, Table 2), varying from 3.2 (TKS201) to 7.5 (TKS203) at the beginning of the experiments, and from 2.9 (TKS201) to 5.0 (PC500) at the end, after 4 h of
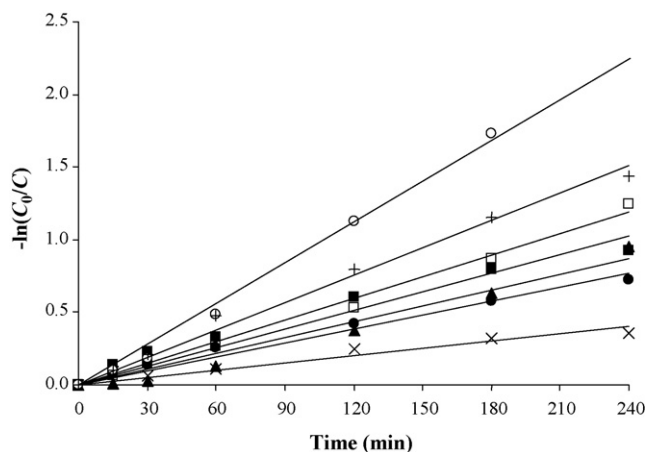

Fig. 2. First-order linear transform $\ln(C_0/C) = f(t)$ for phenol degradation with different TiO$_2$ in suspension (1 g/l): P25 (□), Millennium PC10 (■), PC50 (▲), PC500 (×), Tayca JA1 (+), TKS201 (●) and TKS203 (○) as a function of time. Light intensity of 550 W/m^2.

illumination. Thus, phenol was never in its dissociated state. It was also observed that the pH was decreasing for all samples during phenol degradation experiments. The surface of the two TiO$_2$ with an acidic IEP, Tayca JA1 and TKS203 (Table 1), was negatively charged during the experiments because the pH was always above their IEP, whereas the surface of the five other TiO$_2$ samples was more or less positively charged.

It can be observed in Fig. 1 (trace –) that there is not direct phenol photolysis during the experiments. Since only the soluble phenol concentration was measured and not the one adsorbed on TiO$_2$ surface, it is difficult to dissociate the influence of TiO$_2$ on both adsorption and photodegradation processes after the illumination (time 0–240 min of Fig. 1).

Nevertheless, as observed in Fig. 2 and Table 3, the phenol disappearance after illumination follows an apparent first-order kinetic with a good global correlation coefficient R^2 for all TiO$_2$ types. The two catalysts having the highest degradation kinetics are those with a very acidic IEP, Tayca JA1 (Fig. 1, trace +) and TKS203 (Fig. 1, trace ○) (Table 3), although they have a very different A_{BET} (9 m^2/g for JA1 and 241 m^2/g for TKS203) and aggregate size (9200 nm for JA1 and 200 nm for TKS203). This

Table 4
Total organic carbon removal and pH evolution during phenol degradation and phenol adsorbed after 1 h in the dark for all TiO$_2$ types

Time (min)	TiO$_2$ samples						
	P25	TKS 203	PC50	TKS 201	PC500	PC10	JA1
−60							
TOC (ppm)	36.0	36.0	36.0	36.0	36.0	36.0	36.0
pH	4.6	7.5	4.3	3.2	6.0	5.7	5.6
0							
% Phenol adsorbed	17.8	13.2	17.5	9.7	12.4	12.8	12.1
TOC (ppm)	35.2	33.9	35.6	33.8	35.9	35.2	35.1
pH	4.4	7.2	4.3	3.2	6.0	5.6	5.5
240							
TOC (ppm)	19.1	23.1	23.2	25.8	28.2	29.4	32.0
pH	4.1	4.8	4.1	2.9	5.0	3.9	3.8
% TOC removal	46.9	35.8	35.5	28.5	21.8	18.4	11.0

means that the A_{BET} and aggregate size cannot be correlated with the rate of phenol photocatalytic degradation by TiO_2. Although the phenol dark adsorption onto TiO_2 is not enhanced by a negative TiO_2 surface, the overall process seems to be influenced by electrostatic attraction and repulsion effects, as it was already observed for other compounds [15,16,37]. Another explanation for the high photoactivity of the TKS203 could be related to the high pH observed during the experiment (from 7.5 to 4.8), leading to a higher OH^- ions concentration, and therefore a higher $OH^\bullet$ radical production. On the other hand, the high activity of the JA1 could also be explained by its optical properties. Indeed, as the TiO_2 JA1 has the largest measured particles size (180 nm) and the largest aggregates radius (9200 nm) of all the TiO_2 investigated, it should have a lower radiation scattering in the UV region, and therefore a higher photoactivity than the other TiO_2, as already observed [29,30].

The two neutral catalysts with the highest A_{BET} (PC500 and TKS201) present the lowest degradation kinetics (Table 3), showing that a large surface area is not always necessarily an advantage to degrade a pollutant with a weak adsorption onto TiO_2, as previously reported [16,38–40]. The poor activity observed for TiO_2 PC500 and TKS201 could be explained by an inappropriate crystallinity due to their very small particle size (see Table 1), which induces a smaller lifetime for the photogenerated electrons and holes, as well as a consequently higher recombination rate [39]. The poor phenol adsorption onto the different TiO_2 could also partially explain why its degradation is not better with TiO_2 having a large A_{BET}.

If one compares the apparent first-order rate constant k determined for phenol disappearance (Table 3), the following activity pattern can be obtained: TKS203 > JA1 > P25 > PC10 > PC50 > TKS201 > PC500. However, if one considers the rate of TOC disappearance (Table 4), the classification is totally different: P25 > TKS203 > PC50 > TKS201 > PC500 > PC10 > JA1.

All TiO_2 with small A_{BET} are clearly disadvantaged for TOC removal. The TiO_2 with the smallest A_{BET}, PC10 (10 m^2/g) and JA1 (9 m^2/g) present, respectively, only 18.4 and 11.0% of TOC disappearance after 4 h of illumination, whereas the TOC disappearance was higher than 20% for PC500 and TK201 (Table 4).

These differences can be explained if one considers the intermediates involved in the reaction before the total mineralization of organic carbon to CO_2.

Three intermediate products were detected in the solution: hydroquinone (HQ), benzoquinone (BQ) and catechol (CA). While BQ was found with all the seven catalysts, HQ was detected with only five (JA1, PC 10, PC50, P-25 and TKS203), and CA was detected with two (JA1 and PC10). However, this observation cannot be related to a difference in the reaction mechanism, which would vary with the nature of the photocatalyst, but rather to the difference in the total surface exposed. Indeed, CA has an important adsorption constant [38], whereas the one of HQ is negligible [41]. The catalysts with a medium or a large surface area (P-25, PC50, PC500, TKS201 and TKS203) most probably totally re-adsorb all the CA
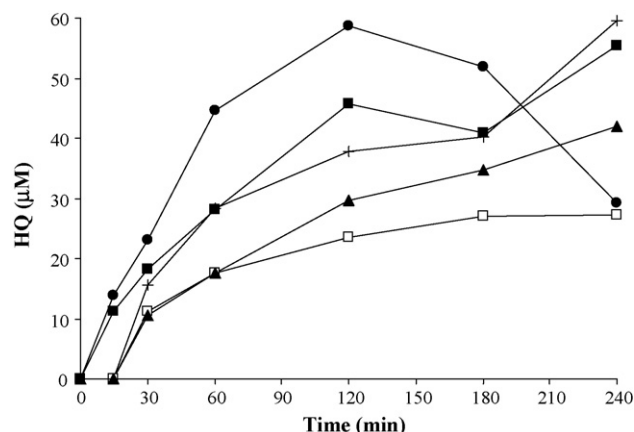

Fig. 3. Evolution of hydroquinone during phenol degradation experiments with different TiO_2 in suspension (1 g/l): P25 (□), Millennium PC10 (■), PC50 (▲), Tayca JA1 (+) and TKS201 (●) as a function of time. Light intensity of 550 W/m^2.

produced as soon as they appear in the solution. By contrast, because of their lower total surface exposed, the photocatalysts JA1 and PC10 cannot adsorb all the CA produced despite their high-adsorption constant. The lack of detection of HQ with catalysts PC500 and TKS 201 could be explained by a slow rate of reduction of BQ to HQ, and/or by an elevated degradation rate of HQ in comparison with phenol.

Fig. 3 shows the HQ concentration evolution during phenol degradation experiments. The concentration of this intermediate after 4 h of illumination is well correlated with the pattern of TOC degradation (Fig. 3 and Table 4). Samples with small A_{BET} (PC10 and JA1) present a final HQ concentration twice as much as the one obtained with the best catalyst for TOC removal (P25).

Due to the many intermediate products generated during the long photodegradation process, a large number of adsorption sites are required not only for the initial pollutant degradation, but also for the degradation of all its intermediates. Therefore, it can be easily conceived that the higher the specific area, the higher the efficiency in destroying all the intermediate products. Thus, CO_2 should be more rapidly formed with catalysts with a large A_{BET} However, the pattern obtained for TOC disappearance does not follow exactly the order of specific areas. P25 (56 m^2/g) appears more active than all samples, included TiO_2 with A_{BET} larger than 200 m^2/g, and PC50 (50 m^2/g) appears more active than TKS201 and PC500.

This observation could be explained by a 'quantum size effect' [42]. When the particles become too small, there is a 'blue shift' with an increase of the band gap energy detrimental to the near UV-photon absorption, and an increase of the electron–hole recombination. A too high specific surface area is therefore not advantageous for an optimum efficiency. The better P25 activity could also be explained by its crystallographic structure, 70% anatase–30% rutile. Generally, anatase is considered to be the photoactive form, while rutile is considered to have low photocatalytic activity. It has been shown in numerous studies that there is a positive interaction of anatase and rutile TiO_2 particles of Degussa P25, which enhances the electron–hole separation and increases the total
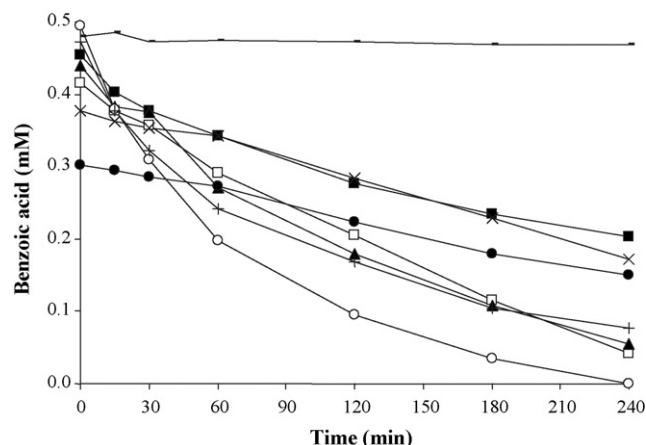
Fig. 4. Photodegradation of benzoic acid (0.5 mM) with different TiO$_2$ in suspension (1 g/l): P25 (□), Millennium PC10 (■), PC50 (▲), PC500 (×), Tayca JA1 (+), TKS201 (●), TKS203 (○) and without TiO$_2$ addition (–) as a function of time. Light intensity of 550 W/m^2.

photoefficiency [43]. The existence of a synergistic effect through the contact between anatase and rutile particles was proven [10], yet the exact conditions necessary for the synergistic phenomena to occur remain unclear to date.

3.2. Benzoic acid (BA)

Fig. 4 shows the BA concentration evolution as a function of the time during experiments with seven different catalysts, and the effect of the light under the same experimental conditions previously described for phenol experiments. Unlike phenol, it appears that, with exception of TKS203, the benzoic acid adsorption onto TiO$_2$ is strongly correlated with the A_{BET} of the TiO$_2$ samples. Indeed, the TiO$_2$ with the smallest A_{BET}, PC10 (10 m^2/g) and JA1 (9 m^2/g), present, respectively, only 9.2 and 5.5% of benzoic acid adsorbed after 1 h of contact, whereas the benzoic acid adsorbed was 24.5% for PC500 (335 m^2/g) and 39.6% for TKS201 (214 m^2/g). Moreover, the TiO$_2$ with medium A_{BET}, about 50 m^2/g (P25 and PC50), present an intermediate adsorption capacity.

Table 5
Apparent first-order rate constant k for benzoic acid disappearance with the different TiO$_2$ samples and their corresponding global correlation coefficient R^2 value

	TiO$_2$ samples						
	TKS 203	JA1	PC50	P25	PC10	PC500	TKS 201
k (min^{-1})	0.867	0.487	0.488	0.401	0.217	0.176	0.168
R^2	0.98	0.97	0.99	0.98	0.96	0.96	0.98

This difference in adsorption behaviour with phenol could be partially explained by the different adsorption mode of the two compounds. Robert et al. [34] demonstrated that organic acids adsorb very fast onto TiO$_2$ via titanium carboxylate formation, unlike phenols, which are poorly adsorbed and lead to Ti-phenolate adsorbates. Nevertheless, the benzoic and phenolic compound adsorption onto TiO$_2$ is a complex mechanism governed by several parameters, and the reasons why only some kinds of adsorption are correlated with the TiO$_2$ A_{BET} have yet not been elucidated.

It was not possible to quantify the adsorbed benzoic acid onto TKS203 because before illumination TiO$_2$ aggregates filtration was hindered by their small size. Nevertheless, after 30 min of illumination due to the agglomeration of TiO$_2$ particles, the filtered BA solution became clear, so that HPLC and TOC measurements could then be realized as for the other TiO$_2$ samples.

As for phenol, kinetics of BA disappearance are of an apparent first order. The rate constant values are listed in Table 5.

Despite the photocatalytic degradation kinetics of a compound is often correlated with its adsorption capacity, this behaviour was not observed for BA degradation. Indeed, TiO$_2$ PC500 and TKS201, which adsorbed the highest quantity of BA, present very slow degradation kinetics in comparison with other TiO$_2$ samples (see Fig. 4 and Table 6). The surface of these catalysts seems to be totally saturated by BA and the reaction intermediates, which do not allow a further degradation of the BA remained in the solution. In the case of

Table 6
Total organic carbon removal and pH evolution during BA degradation and BA adsorbed after 1 h in the dark for all TiO$_2$ type

Time (min)	TiO$_2$ samples						
	P25	TKS 203	PC50	TKS 201	PC500	PC10	JA1
−60							
TOC (ppm)	42.0	42.0	42.0	42.0	42.0	42.0	42.0
pH	3.6	4.4	3.6	3.7	2.8	3.6	3.5
0							
% BA adsorbed	16.9	N.D	12.1	39.7	24.5	9.2	5.5
TOC (ppm)	39.6	42.0	40.9	35.9	40.6	42.0	42.0
pH	3.6	4.5	3.6	3.8	2.9	3.6	3.6
240							
TOC (ppm)	14.7	16.4	17.6	20.4	28.3	32.1	35.3
pH	3.8	4.7	3.6	3.8	2.8	3.5	3.3
% TOC removal	64.9	61.0	58.2	51.5	32.5	23.5	16.1

N.D.: not determined.

well-adsorbing organic pollutants with poor degradation rates, it was proposed that the inhibition of the photocatalytic degradation occurs either via blockage of reaction sites on TiO_2 surface or through their action as locations for surface recombinations of photogenerated holes and electrons [44].

As observed for phenol degradation, the two catalysts with a very acidic IEP (Tayca JA1 and TKS203) have the highest initial rate of degradation (after 1 h of illumination), and it seems that the photodegradation is also influenced by electrostatic attraction and repulsion effects. Nevertheless, after 4 h of illumination, TiO_2 P25 and PC50 present higher percentage of benzoic acid disappearance than JA1. This observation can be explained by a higher accumulation of reaction intermediates in the solution during the process with JA1, compared to P25 and PC50, which could be due to its smaller A_{BET}. A competition between the intermediates and BA for degradation takes place and the rate of BA disappearance slows down.

TOC removal and pH evolution during BA degradation for all TiO_2 types are presented in Table 6.

The pattern obtained for TOC removal is the same as the one of phenol: P25 > TKS203 > PC50 > TKS201 > PC500 > PC10 > JA1. As observed for phenol, it seems that smaller A_{BET} TiO_2 are disadvantaged, and that there is an optimal value of A_{BET} for TOC removal. Nevertheless, all the TiO_2 samples present a higher TOC removal for BA degradation than for phenol degradation (for example 64.9% of TOC removal for BA vs. 46.9% for phenol with TiO_2 P25).

Three aromatic organic compounds – *ortho*-, *meta*- and *para*-hydroxybenzoic acids – were identified as intermediates during benzoic acid degradation, as previously observed during photocatalytic oxidation of BA by TiO_2 [45,46]. The evolution of HBA concentration during BA degradation experiments with the different TiO_2 is shown in Fig. 5.

It can be observed that higher concentrations of intermediates were found in the solution with TiO_2 having small A_{BET} during benzoic acid degradation experiments (Fig. 5, PC10, traces ■, and JA1, traces +).
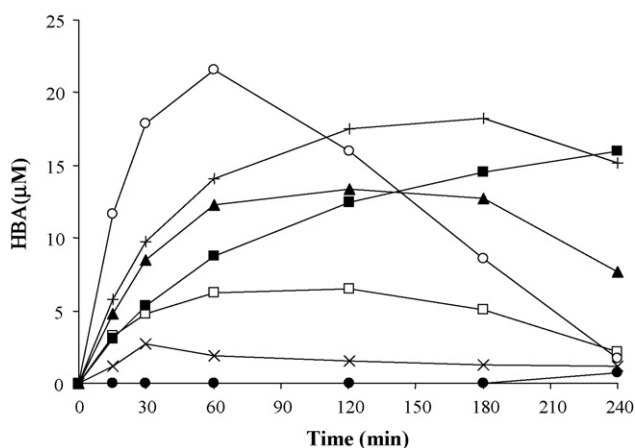

Fig. 5. Evolution of 4-hydrobenzoic acid concentration during benzoic acid degradation with different TiO_2 in suspension (1 g/l): P25 (□), Millennium PC10 (■), PC50 (▲), PC500 (×), Tayca JA1 (+), TKS201 (●) and TKS203 (○) as a function of time. Light intensity of 550 W/m².
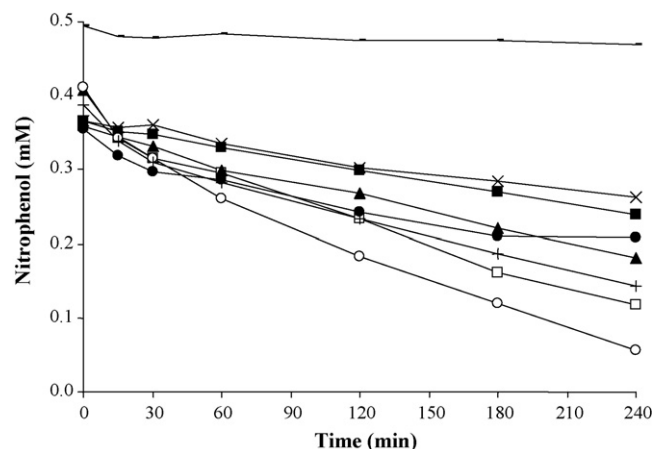

Fig. 6. Photodegradation of 4-nitrophenol (0.5 mM) with different TiO_2 in suspension (1 g/l): P25 (□), Millennium PC10 (■), PC50 (▲), PC500 (×), Tayca JA1 (+), TKS201 (●), TKS203 (○) and without TiO_2 addition (–) as a function of time. Light intensity of 550 W/m².

The pH shifted only slightly during BA photodegradation and always remained under its pK_a (4.19) for all the TiO_2 samples but TKS203 (pH from 4.4 to 4.7) (see Table 6). Thus, BA was always protonated, except in experiments with TKS203. It seems that acidic TiO_2 with negative surface charge are more efficient catalysts than neutral ones for BA degradation, even when the BA is partially deprotonated and should have an electrostatic repulsion with the catalyst. As for phenol, this could be explained by the higher concentration of OH^- ions in solution, i.e. the higher probability to form $OH^\bullet$ radical, due to the higher pH value of 4.5 for TKS203 before illumination, compared to all the other TiO_2 (from 2.9 for TKS201 to 3.8 for PC500) (Table 6).

3.3. 4-Nitrophenol (NP)

Fig. 6 shows NP concentration evolution as a function of time during photocatalytic experiments with seven different catalysts, and the effect of the light under the same experimental conditions as previously described for phenol. Their respective first-order rate constants are summarized in Table 7. The evolution of TOC and pH are shown in Table 8.

The trends obtained for NP adsorption and photodegradation, TOC removal and the evolution of pH are very similar to those obtained for phenol (see Figs. 1 and 6, Tables 4 and 8). NP is adsorbed onto TiO_2 via the same mechanism as phenol, i.e. formation of phenolate and/or by a flat adsorption of the aromatic ring parallel to the TiO_2 surface [34]. There is no

Table 7
Apparent first-order rate constant k for nitrophenol disappearance with the different TiO_2 samples and their corresponding global correlation coefficient R^2 value

	TiO₂ samples						
	TKS 203	P25	JA1	PC50	TKS 201	PC10	PC500
k (min⁻¹)	0.418	0.264	0.252	0.211	0.158	0.104	0.0859
R^2	0.99	0.98	0.98	0.93	0.87	0.99	0.99

Table 8
Total organic carbon removal and pH evolution during NP degradation and NP adsorbed after 1 h in the dark for all TiO$_2$ types

Time (min)	TiO$_2$ samples						
	P25	TKS 203	PC50	TKS 201	PC500	JA1	PC10
−60							
TOC (ppm)	36.0	36.0	36.0	36.0	36.0	36.0	36.0
pH	4.4	6.3	4.3	2.9	5.6	5.2	5.0
0							
% NP adsorbed	28.2	17.8	18.6	29.1	26.7	22.5	26.8
TOC (ppm)	34.6	35.0	33.5	34.2	35.0	34.7	35.5
pH	4.3	6.4	4.3	2.9	5.5	5.2	4.8
240							
TOC (ppm)	18.6	22.8	25.0	27.6	29.4	30.6	30.7
pH	3.6	4.0	3.6	2.8	4.2	3.5	4.2
% TOC removal	48.4	36.8	30.6	23.4	18.2	15.0	14.9

correlation between adsorption or photodegradation and the A_{BET} (Fig. 6). The pH was always below the pK_a of NP (7.15), varying from 2.9 (TKS201) to 6.3 (TKS203) at the beginning of the experiments, and from 2.9 (TKS201) to 4.2 (PC500) at the end after 4 h of illumination. Thus, NP was never in the dissociate state. We also observed a decrease on the pH value for all samples during NP degradation. The best NP degradation kinetics is obtained with TiO$_2$ TKS203, as previously observed for phenol and BA degradation. TiO$_2$ catalysts with high A_{BET} do not necessarily present better kinetics than TiO$_2$ samples with small A_{BET} (Table 7).

TiO$_2$ samples with small A_{BET} present poor TOC removal, and P25 has the best percentage of TOC removal of all the catalysts (Table 8). Thus the nitro group does not seem to play a determinant role in the interaction with TiO$_2$.

Nevertheless, NP showed a higher percentage of adsorption on TiO$_2$ than phenol (Tables 3 and 7), although its kinetics of degradation was slower (Figs. 1 and 6). The K_{ow} value, which reflects the trend for these molecules to remain in or escape from water, is higher for the NP than for phenol (Table 2) and could explain the higher adsorption of NP on TiO$_2$, as it was already observed recently for other phenolic compounds [23].

The difference in the degradation kinetics could be explained by the Hammett constant σ of the compounds. Indeed, the photodegradation rates are accelerated by electron-donating groups and retarded by electron-withdrawing groups [22]. Due to the electron-withdrawing –NO$_2$ group, the electron density over the aromatic ring is higher for phenol than NP (see Table 2); the electron-donating capacity is thus lower for NP than phenol, which can explain its slower degradation kinetic.

As intermediate products of the NP photocatalytic degradation, HQ and a trace amount of BQ were found. This observation is in agreement with previous studies [47–49] that identified HQ as the primary product of the NP transformation via photocatalysis. The nitrogroup in nitroaromatics is an excellent leaving group, which can be easily eliminated, favouring the electrophilic substitution of OH$^\bullet$ radicals at the *para* position with respect to the hydroxyl group [47].

3.4. 4-Hydroxybenzoic acid (HBA)

Fig. 7 shows the HBA concentration evolution as a function of time during photocatalytic experiments with seven different catalysts, and the effect of the light under the same experimental conditions as previously described for phenol. Their respective first-order rate constants are listed in Table 9. The evolution of TOC and pH during the experiments is shown in Table 10.

Results of HBA adsorption and degradation present a quite different figure than the three other compounds. First, as shown in Fig. 7, the adsorption of HBA with exception of TKS203 is correlated with the A_{BET} as already observed for BA, for which the same filtration problem occurred. However, unlike for phenol, BA and NP degradation, degradation kinetics of HBA are correlated with the A_{BET}. Indeed, the three catalysts with the higher A_{BET} – TKS201, TKS203, and PC500 – present the highest HBA degradation kinetics (Table 9).

Moreover, the catalyst presenting the highest percentage of TOC removal after 4 h of illumination (PC500) has the highest A_{BET} (Table 10). It seems that the overall process is first
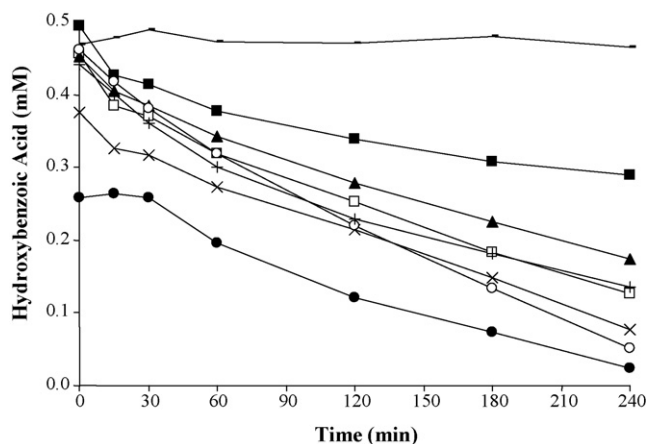

Fig. 7. Photodegradation of 4-hydroxbenzoic acid (0.5 mM) with different TiO$_2$ in suspension (1 g/l): P25 (□), Millennium PC10 (■), PC50 (▲), PC500 (×), Tayca JA1 (+), TKS201 (●), TKS203 (○) and without TiO$_2$ addition (–) as a function of time. Light intensity of 550 W/m^2.

Table 9
Apparent first-order rate constant k for HBA disappearance with the different TiO$_2$ samples and their corresponding global correlation coefficient R^2 value

	TiO$_2$ samples						
	TKS 203	TKS 201	PC500	P25	JA1	PC50	PC10
k (min^{-1})	0.400	0.388	0.355	0.314	0.307	0.240	0.151
R^2	0.99	0.95	0.96	0.99	0.99	0.98	0.75

governed by the specific area of the catalyst and then to a lesser extent by their IEP.

For the 4-HBA, the chemisorption is fast via titanium carboxylate, as for BA, but also via phenolate formation. It seems that this bifunctional compound gives a bidentate [34,41,50]. This different mode of adsorption could explain the difference of behaviour.

3.5. Comparison of organic degradation kinetics as a function of TiO$_2$ types

In order to address the importance of the TiO$_2$ characteristics depending on the nature of the pollutant, a comparison of the adsorption and the degradation kinetics of the four previously investigated compounds with TiO$_2$ catalysts which have approximately the same A_{BET} was made. Concerning the two catalysts with an average A_{BET} (50 m^2/g), P25 and PC50, after 4 h of illumination, a higher organic disappearance was observed with P25 than with PC50 for all compounds. The only difference in the TiO$_2$ catalyst characteristics is a 70% anatase–30% rutile for P25 and a 100% anatase crystalline phase for PC50. Therefore, the difference of activity towards the organic substances could most probably be attributed to the different crystalline structure.

The degradation kinetics of the four compounds with the two TiO$_2$ catalysts which have a small A_{BET} (~10 m^2/g), PC10 and JA1 was observed (Tables 3, 5, 7 and 9). These two catalysts have very similar A_{BET} but very different surface charges (see Table 1). It can be observed that JA1 TiO$_2$, having a very acidic IEP, presents a much better photoactivity than PC10, which

have an IEP of 5.7. Thus, electrostatic attraction seems to be the determining parameter for the photodegradation process. Nevertheless, as JA1 has larger aggregates (9200 nm) than PC10 (1000 nm) at neutral pH, different optical properties could also partially explain the better photoactivity of the JA1.

The degradation of the four compounds with the three TiO$_2$ catalysts which have a large A_{BET} (>200 m^2/g), TKS201, TKS203 and PC500 was observed (Tables 3, 5, 7 and 9). As for the small A_{BET}, the catalyst with an acidic IEP (TKS203) has a better photoactivity than the others on all model pollutants. In the case of TKS203, the fast degradation kinetics could be attributed to either electrostatic attraction, or to a higher OH$^\bullet$ production due to a higher pH observed during experiments with TKS203 in comparison with the experiments with TKS201 and PC500.

The A_{BET} is not a crucial property for primary compounds degradation. The unique exception is with HBA, which is degraded faster with TKS203, TKS201 and PC500, having a large A_{BET} (Table 9). However, total organic mineralization is disadvantaged with TiO$_2$ samples having small A_{BET} (PC10 and JA1) (Tables 4, 6, 8 and 10). A_{BET} of TiO$_2$ samples are strongly correlated with their particle size (Table 1), and an optimum particle size around ~30 nm (P25 and PC50) was found, for which an efficient TOC removal was observed.

Compounds with a carboxyl group (BA and HBA) and those without (phenol and NP) exhibit different behaviour during adsorption and degradation experiments that can neither be explained with their σ nor with their K_{ow} values. Indeed, phenol, with the lowest σ value of the four compounds, and therefore, the highest electron-donating capacity (Table 2), presents slower degradation kinetics than BA or HBA with the majority of TiO$_2$ samples. Moreover, the adsorption of compounds having a carboxyl group is not correlated with their K_{ow} values. BA and HBA present approximately the same K_{ow} as phenol (Table 2) but were more adsorbed onto TiO$_2$ with a large A_{BET}. This lack of correlation could be explained by taking into account the chemical interactions in the substrate adsorption onto TiO$_2$ surface, and not only the removal from the aqueous solution because of hydrophobicity. The higher degradability of

Table 10
Total organic carbon removal and pH evolution during HBA degradation and HBA adsorbed after 1 h in the dark for all TiO$_2$ types

Time (min)	TiO$_2$ samples						
	PC500	TKS 203	PC50	P25	TKS 201	JA1	PC10
−60							
TOC (ppm)	42.0	42.0	42.0	42.0	42.0	42.0	42.0
pH	2.9	4.8	4.1	3.9	3.9	3.9	4.0
0							
% HBA adsorbed	24.8	N.D.	9.5	8.9	48.5	11.8	1.3
TOC (ppm)	40.3	42.0	34.2	42.0	39.4	42.0	41.5
pH	2.7	4.8	3.9	3.7	3.6	3.7	4.0
240							
TOC (ppm)	30.3	23.7	14.5	37.9	25.4	24.8	33.8
pH	2.6	4.6	3.8	3.7	3.5	3.6	3.7
% TOC removal	65.4	43.7	41.0	39.5	28.0	19.5	9.8

N.D.: not determined.

BA and HBA could be due to the presence of a carboxylic group which can easily react with holes h^+ via a photo-Kolbe reaction (Eq. (3)) [51]:

$$RCOO^- + h^+ \rightarrow R^\bullet + CO_2 \qquad (3)$$

The aggregate size influence on the TiO_2 activity is difficult to evaluate. This might be attributed to its pH dependence, and therefore, its fluctuating value during the experiments. Nevertheless, as the aggregate size is proportional to the TiO_2 optical properties and therefore with their photoactivities, a more detailed study of its influence should be investigated.

TiO_2 Degussa P25 was the best of the neutral (IEP approximately 7) TiO_2 samples for the primary compounds degradation and the best of all for the total organic mineralization. This high efficiency is certainly due to its average particle size ($\sim$30 nm) and to its mixed crystalline structure (70% anatase–30% rutile) (Table 1).

4. Conclusion

The main physicochemical characteristics of seven commercial TiO_2 powders were studied and tested in order to correlate them with the TiO_2 catalysts photoactivities. The crystalline phase, the particle size, the aggregate size, the specific surface area (A_{BET}) and the isoelectric point (IEP) were determined for each sample and correlated with organic degradation kinetics. The results showed that IEP seems to influence significantly organic degradation. Indeed, TiO_2 catalysts with an acidic IEP accelerate organic compounds degradation. This is most likely due to electrostatic attraction–repulsion effects between TiO_2 and the targeted contaminant, although other parameters, such as the pH or the aggregate size, could also play an important role in the photocatalytic process. A_{BET} strongly influences the adsorption and the degradation kinetics of strongly adsorbed organics, while it had no effect on weakly adsorbed pollutants. However, a non-linear correlation of A_{BET} with the total organic carbon (TOC) removal was observed for all organic compounds. There is an optimum A_{BET} value and an optimum particle size for TOC removal. The crystalline structure is an important parameter for an efficient photoactivity of the TiO_2 catalyst in organic pollutant degradation. The mixed anatase–rutile (75–25%) Degussa P25 TiO_2 sample was found to be more efficient than samples containing pure anatase.

Depending on the nature of the contaminant, different TiO_2 properties/characteristics have to be considered regarding the TiO_2 efficiency on water treatments. Consequently, it is difficult to draw a general conclusion on which TiO_2 photocatalyst is the most suitable for water decontamination. Indeed, many factors are involved and interfere in the testing of catalyst behaviour during the degradation of a contaminant. A thorough comparison of TiO_2 activity should include reactions with several different pollutants under varied experimental conditions. However, in our case, the mixed P25 TiO_2 presented the best compromise.

References

[1] D.F. Ollis, E. Pelizzetti, N. Serpone, in: N. Serpone, E. Pelizzetti (Eds.), Photocatalysis: Fundamentals and Applications, Wiley Interscience, New York, 1989.
[2] H. Gerischer, Electrochim. Acta 40 (1995) 1277–1281.
[3] A. Mills, S. Le Hunte, J. Photochem. Photobiol. A: Chem. 108 (1997) 1–35.
[4] M. Kaneko, I. Okura, in: M. Kaneko, I. Okura (Eds.), Photocatalysis: Science and Technology, Kodansha-Springer Verlag, Tokyo, 2002.
[5] C.-C. Wang, J.Y. Ying, Z. Zhang, Nanostruct. Mater. 9 (1997) 583–586.
[6] Z. Zhang, C.-C. Wang, R. Zakaria, J.Y. Ying, J. Phys. Chem. B 102 (1998) 10871–10878.
[7] A.J. Maira, K.L. Yeung, C.Y. Lee, P.L. Yue, C.K. Chan, J. Catal. 192 (2000) 185–196.
[8] C.B. Almquist, P. Biswas, J. Catal. 212 (2002) 145–156.
[9] O. Carp, C.L. Huisman, A. Reller, Prog. Solid State Chem. 32 (2004) 33–177.
[10] T. Ohno, K. Sarukawa, K. Tokieda, M. Matsumura, J. Catal. 203 (2001) 82–86.
[11] R.I. Bickley, T. Gonzalez-Carreno, J.S. Lees, L. Palmisano, R.J.D. Tilley, J. Solid State Chem. 92 (1991) 178–190.
[12] M. Inagaki, Y. Nakazawa, M. Hirano, Y. Kobayashi, M. Toyoda, Int. J. Inorg. Mater. 3 (2001) 809–811.
[13] M. Toyoda, Y. Nanbu, Y. Nakazawa, M. Hirano, M. Inagaki, Appl. Catal. B: Environ. 49 (2004) 227–232.
[14] J. Cunningham, P. Sedlak, Photocatalytic Purification and Treatment of Water and Air, 1993, pp. 67–81.
[15] C. Guillard, H. Lachheb, A. Houas, M. Ksibi, E. Elaloui, J.-M. Herrmann, J. Photochem. Photobiol. A: Chem. 158 (2003) 27–36.
[16] A. Piscopo, D. Robert, J.V. Weber, Appl. Catal. B: Environ. 35 (2001) 117–124.
[17] J.M. Tseng, C.P. Huang, Water Sci. Technol. 23 (1991) 377–387.
[18] J.C. D'Oliveira, C. Minero, E. Pelizzetti, P. Pichat, J. Photochem. Photobiol. A: Chem. 72 (1993) 261–267.
[19] L. Amalric, C. Guillard, E. Blanc-Brude, P. Pichat, Water Res. 30 (1996) 1137–1142.
[20] B. Sangchakr, T. Hisanaga, K. Tanaka, J. Photochem. Photobiol. A: Chem. 85 (1995) 187–190.
[21] W.Z. Tang, H. An, Chemosphere 31 (1995) 4157–4170.
[22] S. Parra, C. Pulgarin, J. Olivero, L. Pacheco, Appl. Catal. B: Environ. 43 (2003) 293–301.
[23] M. Lapertot, P. Pichat, S. Parra, C. Guillard, C. Pulgarin, J. Environ. Sci. Health A: Toxicol. Hazard. Subst. Environ. Eng. 41 (2006) 1009–10025.
[24] E. Pelizzetti, Sol. Energy Mater. Sol. Cells 38 (1995) 453–457.
[25] J.-M. Herrmann, C. Guillard, P. Pichat, Catal. Today 17 (1993) 7–20.
[26] K.-H. Wang, Y.-H. Hsieh, C.-H. Wu, C.-Y. Chang, Chemosphere 40 (2000) 389–394.
[27] K.-H. Wang, Y.-H. Hsieh, M.-Y. Chou, C.-Y. Chang, Appl. Catal. B: Environ. 21 (1999) 1–8.
[28] V. Loddo, M. Addamo, V. Augugliaro, L. Palmisano, M. Schiavello, E. Garrone, J. Am. Chem. Soc. 52 (2006) 2565–2574.
[29] D. Vione, C. Minero, V. Maurino, M.E. Carlotti, T. Picatonotto, E. Pelizzetti, Appl. Catal. B 58 (2005) 79.

[30] C. Minero, D. Vione, Appl. Catal. B: Environ. 67 (2006) 257–269.

[31] D. Gumy, C. Morais, P. Bowen, C. Pulgarin, S. Giraldo, R. Hajdu, J. Kiwi, Appl. Catal. B: Environ. 63 (2006) 76–84.

[32] D. Gumy, A.G. Rincon, R. Hajdu, C. Pulgarin, Sol. Energy 80 (2006) 1376–1381.

[33] J. Cunningham, P. Sedlak, Catal. Today 29 (1996) 309–315.

[34] D. Robert, J.V. Weber, S. Parra, C. Pulgarin, A. Krzton, Appl. Surf. Sci. 167 (2000) 51–58.

[35] A.M. Peiro, J.A. Ayllon, J. Peral, X. Domenech, Appl. Catal. B: Environ. 30 (2001) 359–373.

[36] S. Bekkouche, M. Bouhelassa, N.H. Salah, F.Z. Meghlaoui, Desalination 166 (2004) 355–362.

[37] P. Pizarro, C. Guillard, N. Perol, J.-M. Herrmann, Catal. Today 101 (2005) 211–218.

[38] C. Guillard, J. Disdier, J.-M. Herrmann, C. Lehaut, T. Chopin, S. Malato, J. Blanco, Catal. Today 54 (1999) 217–228.

[39] J.-M. Herrmann, C. Guillard, J. Disdier, C. Lehaut, S. Malato, J. Blanco, Appl. Catal. B: Environ. 35 (2002) 281–294.

[40] S. Malato, J. Blanco, A. Campos, J. Caceres, C. Guillard, J.M. Herrmann, A.R. Fernandez-Alba, Appl. Catal. B: Environ. 42 (2003) 349–357.

[41] U. Stafford, K.A. Gray, P.V. Kamat, J. Phys. Chem. 98 (1994) 6343–6351.

[42] A.J. Nozik, in: D.F. Ollis, H. El-Ekabi (Eds.), Photocatalytic Purification and Treatment of Water and Air, Elsevier, Amsterdam, 1993.

[43] B. Sun, P.G. Smirniotis, Catal. Today 88 (2003) 49–59.

[44] J. Cunningham, S. Srijaranai, in: G.R. Helz, R.G. Zepp, D.G. Crosby (Eds.), Aquatic and Surface Photochemistry, Lewis Publishers, Boca Raton, 1994.

[45] R.W. Matthews, Water Res. 20 (1986) 569–578.

[46] A.H.C. Chan, C.K. Chan, J.P. Barford, J.F. Porter, Water Res. 37 (2003) 1125–1135.

[47] A. Di Paola, V. Augugliaro, L. Palmisano, G. Pantaleo, E. Savinov, J. Photochem. Photobiol. A: Chem. 155 (2003) 207–214.

[48] B. Malinowska, J. Walendziewski, D. Robert, J.V. Weber, M. Stolarski, Appl. Catal. B: Environ. 46 (2003) 441–451.

[49] V. Maurino, C. Minero, E. Pelizzetti, P. Piccinini, N. Serpone, H. Hidaka, J. Photochem. Photobiol. A: Chem. 109 (1997) 171–176.

[50] A. Piscopo, D. Robert, J.V. Weber, J. Photochem. Photobiol. A: Chem. 139 (2001) 253–256.

[51] J.-M. Herrmann, H. Tahiri, C. Guillard, P. Pichat, Catal. Today 54 (1999) 131–141.